Progress In Electromagnetics Research Letters, Vol. 128, 41–47, 2025

PIER Letters

(Received 23 September 2025, Accepted 5 December 2025, Scheduled 13 December 2025)

A Touch Sensing Method Using EIT-Based Microstrip Structure for Interactive Applications

Jiyou Jiang[1] and Jiangtao Huangfu[2,*]

[1]*School of Electrical, Electronic and Computer Engineering, The University of Western Australia*
35 Stirling Highway, Crawley, 6009 Western Australia, Australia
[2]*College of Information Science and Electronic Engineering, Zhejiang University, Hangzhou, China*

ABSTRACT: Touch interaction is an important function in various electronic systems. In this paper, a touch sensing method based on an electromagnetically induced transparency (EIT) microstrip structure is proposed. The design consists of a U-shaped two-port microstrip transmission line with four open stubs oriented in four directions. Two transmission narrow bands are generated by the proposed structure at around 1.8 GHz and 3.5 GHz, corresponding to the EIT effect. When finger-like objects approach the terminals of these open stubs, their transmission characteristics change significantly, as indicated by variations in the S-parameter response. To precisely determine the touch position, a shifting vector method is introduced based on the variations of S-parameters at different touch positions on the board plane. Both simulation and experimental results demonstrate a touch localization accuracy of 94.4% with a spatial resolution of 3 mm. The proposed design offers a low-cost and compact platform that integrates touch interaction and RF communication, showing strong potential for future interactive electronic and communication systems.

1. INTRODUCTION

Electromagnetically induced transparency (EIT) is a technique that used to eliminate the effect of medium on a propagation beam of electronic radiation and always be explained by three energy levels 'coupling' with two incident lights in quantum field. It's mostly used in optical and photon area [1, 2] — by means of a beam of light, a material will be 'transparent' to another light at different frequency. This phenomenon always comes along with slow light effect [3] and applies to optical switching [4].

Such procedure can also be made an analogy into classic field and represented by the RLC coupling circuits, where the EIT phenomenon is generated by coupling and resonating among circuits' components like capacitance and inductance [5–8]. This is because the resonance generated by the intense interference between the electric fields of those close RLC stubs would induce the characteristics of narrow band penetration, namely EIT band. A special RLC coupling circuits design for a microstrip filter is proposed with specifically calculated size. In this way, the microstrip line and those open-stubs are able to replace the RLC structure which can achieve the destructive interference through the near field coupling effect known as EIT. These EIT bands are quite ultra-sensitive to interference of surrounding objects revealed from experiments, thus have the potential to be utilized for sensing [9, 10], confirming movement of electric materials and even traces for applications like gesture recognition.

Recent studies have further extended EIT and Fano resonance mechanisms to practical microwave sensing and integrated RF systems [11–14], demonstrating their potential in multifunctional and cost-efficient interactive applications. More recent works have also explored microstrip-based EIT structures, including single-branch resonators directly coupled to the sensing dielectric and metallic multi-branch units that generate multiband EIT effects [15–17], although these designs generally lack spatial localization capability. In contrast, the present work adopts a transmission-line EIT architecture with four parallel microstrip branches, enabling dual-band sensing and two-dimensional touch-position detection through the proposed shifting-vector method.

In this paper, a more practical U-shaped microstrip structure is adopted after validating the fundamental shifting tendency of the S-parameters when finger-like objects approach the open stubs. Through both simulation and experimental verification, the correlation between the object position and the distinct variations in the S_{21} curves is clearly established, and a shifting vector is introduced to quantitatively describe their mapping relationship. Unlike conventional touch or proximity sensors that rely on additional components, the proposed structure enables interactive sensing without introducing any extra sensor elements, ensuring that the original RF communication performance and other circuit functions remain compatible. This integrated design achieves low-cost, compact, and multifunctional interaction capability, making the proposed EIT-based microstrip structure highly promising for practical applications in touch sensing and gesture recognition during RF signal transmission.

2. THEORY AND ANALYSIS

The design specifications of the proposed structure were defined prior to the theoretical formulation to ensure suitabil-

---

[*] Corresponding author: Jiangtao Huangfu (huangfujt@zju.edu.cn).

doi:10.2528/PIERL25092302

Published by THE ELECTROMAGNETIC ACADEMY

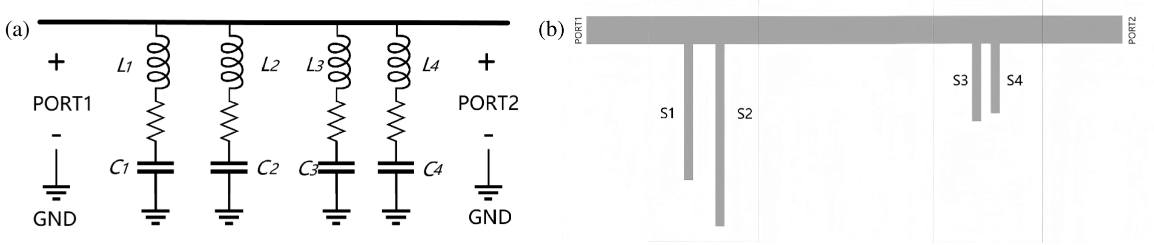

FIGURE 1. Schematic and equivalent form of the proposed structure.

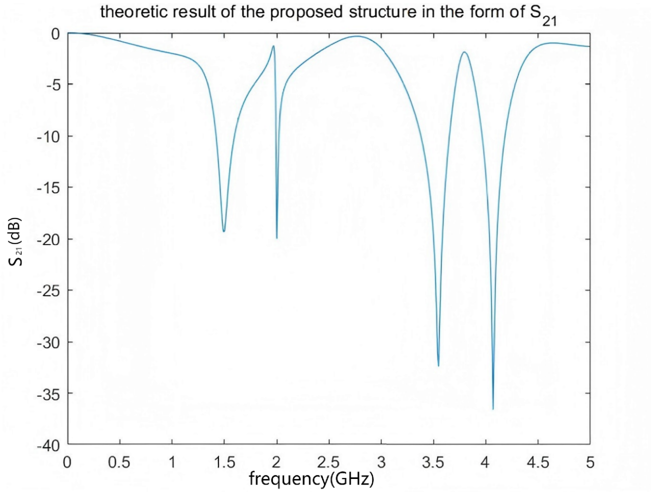

FIGURE 2. $C_1 = 2\,\text{pF}$, $C_2 = 0.1\,\text{pF}$, $C_3 = 0.2\,\text{pF}$, $C_4 = 0.5\,\text{pF}$.

ity for centimeter-scale touch-position sensing. Since the intended interaction distance is on the order of several centimeters, the four parallel microstrip branches were dimensioned accordingly, with lengths in the centimeter range so that localized dielectric loading can produce clearly distinguishable perturbations in the EIT resonances. The two EIT bands were designed to operate in the GHz range, compatible with sub-6-GHz RF communication circuits, and the structure was implemented on a low-cost FR-4 substrate to achieve a practical balance among size, cost, and electromagnetic performance. These specifications enable the proposed microstrip structure to support both signal transmission and interactive sensing, making it suitable for compact wireless and consumer-grade RF systems.

As shown in Figure 1(a), the schematic design of a microstrip structure is given with two EIT bands. Those four RLC series structure are divided into two pairs and each induces a narrow EIT band.

Figure 1(b) shows the structure of microstrip line and open stubs with given size to replace the RLC circuit. The microstrip structure is fabricated on a specific substrate with dielectric constant of $\hat{\epsilon}_r = 2.9$ and thickness of 1 mm. For more detailed parameters, the microstrip line is 5 mm in width and the size of the open stubs are (19.5 mm, 1.5 mm), (25 mm, 1.5 mm), (12.7 mm, 1 mm), (11 mm, 1 mm) in the form of (length, width) for S1, S2, S3, S4 respectively.

In order to describe the performance and transmit capacity of this structure, S_{21} is used to measure the transmission response, which can efficiently represent the transmission loss. More specifically, the closer it is to 0 dB, the less the transmission loss is. The whole structure can be regarded as a microstrip transmission line with four open stubs in parallel and its circuits' parameters can be simply obtained by multiplication of $ABCD$ matrix [18]. By applying the Kirchhoff's current equation to the circuit structure, the analytical S_{21} can be obtained:

$$S_{21} = \frac{Z_0}{AZ_0 + B + CZ_0^2 + DZ_0} \tag{1}$$

where A, B, C, D are those of the whole $ABCD$ matrix. The effect of mutual coupling among stubs is not fully considered in this simplified model, but its impact is relatively small. Figure 2 shows the theoretic S_{21} of the proposed structure in Figure 1(b) simulated by ADS software. It is clear that there are two EIT bands whose peak frequencies are at around 1.8 GHz and 3.8 GHz respectively, which is consistent with the analytical result. The original values of the four stubs' capacitance are shown below the figure.

The capacitance values of the four open stubs, shown in Figure 2, were determined through simulation-based parameter extraction. A full-wave electromagnetic model of the proposed structure was built in CST Microwave Studio, and the corresponding equivalent circuit parameters were obtained by fitting the simulated S-parameters to the analytical $ABCD$-matrix model. This fitting approach ensures that the simplified analytical model accurately reflects the electromagnetic behavior of the structure, including the fringing-field and parasitic effects that are difficult to capture analytically. Hence, the capacitance values used in the analysis represent the effective equivalent capacitances of the stubs rather than purely theoretical values. When capacitive loading occurs near the terminals of the four open stubs, the local capacitance changes significantly due to near-field coupling, resulting in the shift of EIT bands. Moreover, as objects slightly move closer, not only would the EIT peak frequency alter, but also the EIT bandwidth would distinctly change until the EIT effect finally disappears.

To simulate the capacitive loading effect on the structure shown in Figure 1(b), the capacitances of those four open stubs are slightly changed according to their initial values. While the capacitance is changing, the S_{21} wave form is observed at the same time to figure out the basic tendency between the movement of capacitive loading and the shift of EIT bands.

Figure 3 shows the simulation results when capacitive loading is approaching to different open stubs which is represented by the increment of capacitance. In Figure 3(a), when the value of C_1 is increased, the EIT band with peak frequency

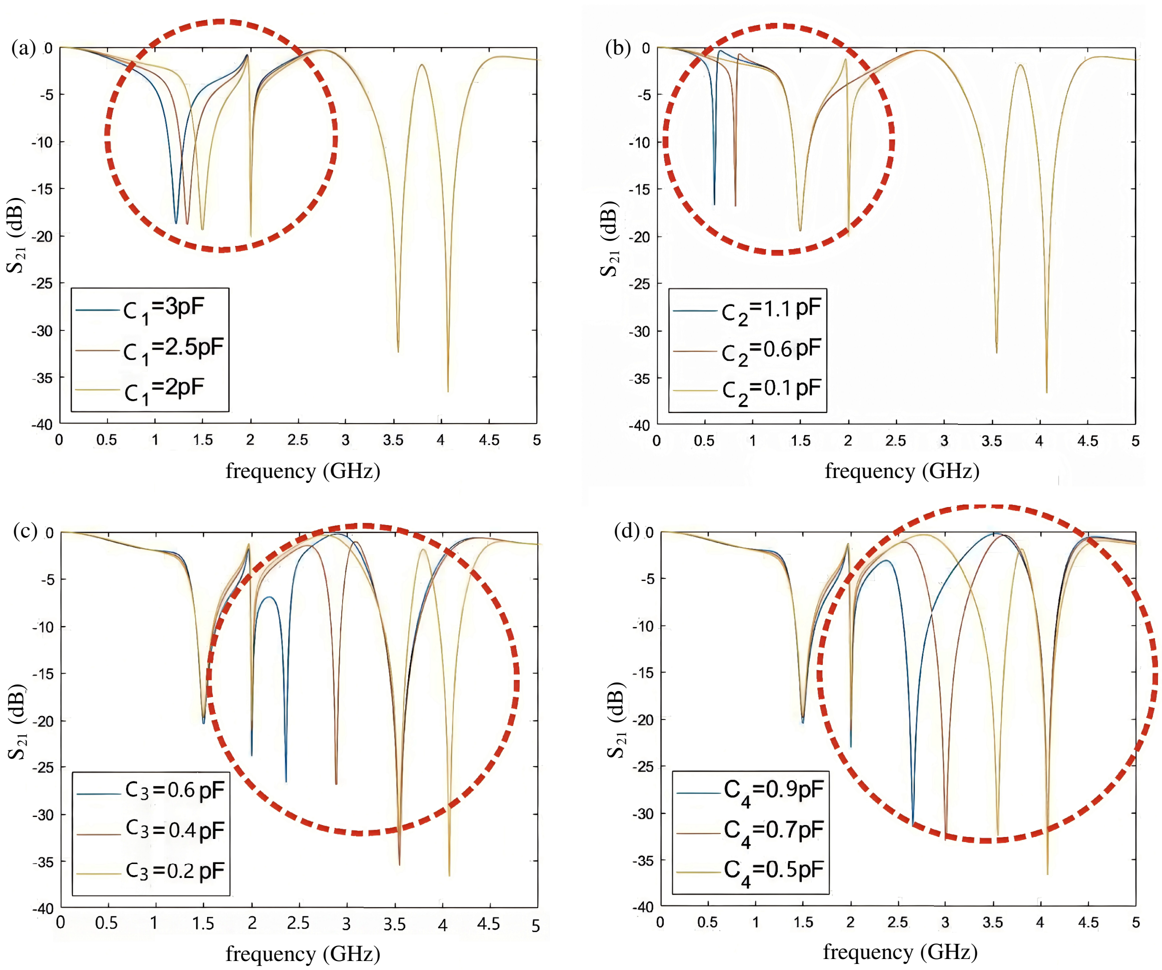

FIGURE 3. The transmission response results of S_{21}. (a) Change the capacitance of C_1. (b) Change the capacitance of C_2. (c) Change thecapacitance of C_3. (d) Change the capacitance of C_4.

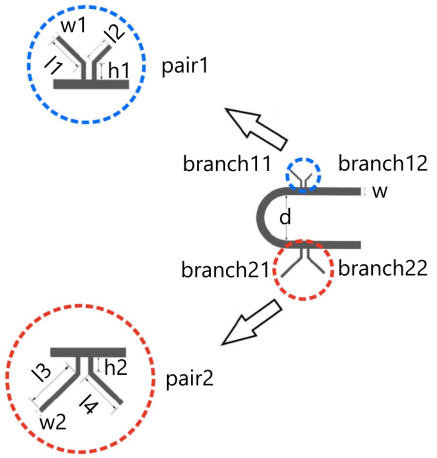

FIGURE 4. The detailed values of the proposed U-designed structure are $w = 5\,\mathrm{mm}$, $w_1 = 1\,\mathrm{mm}$, $w_2 = 1.5\,\mathrm{mm}$, $d = 10\,\mathrm{mm}$, $h_1 = 5\,\mathrm{mm}$, $h_2 = 8\,\mathrm{mm}$, $l_1 = 12.7\,\mathrm{mm}$, $l_2 = 11\,\mathrm{mm}$, $l_3 = 25\,\mathrm{mm}$, $l_4 = 19.5\,\mathrm{mm}$.

around 1.8 GHz would slightly move to lower frequency. In Figure 3(b), when the value of C_2 is increased, the EIT band with peak frequency around 1.8 GHz will significantly shift towards lower frequencies up to 800 MHz

Meanwhile, when the value of C_3 is increased in Figure 3(c), the EIT band with peak frequency around 3.8 GHz will significantly shift towards lower frequencies up to 2.8 GHz. When the value of C_4 is increased in Figure 3(d), the EIT band with peak frequency around 3.8 GHz will slightly shift towards lower frequencies up to 3.5 GHz.

These results demonstrate that the proposed microstrip structure is suitable for sensing applications, since the EIT bands change significantly under capacitive loading. In other words, the variation of the EIT response indicates the presence or movement of nearby capacitive loading.

3. DESIGN AND SIMULATION

A more compact U-design microstrip sensing structure with four open stubs, each bends 45 degrees according to upright, is designed to recognize the movement of finger (representing of capacitive loading) from different orientations. The sensing structure and its detailed size information are shown in Figure 4. One cylinder with 8 mm of radius and 40 mm of height is used to simulate capacitive loading. In order to make an analogy to the movement of finger, the permittivity is set $as\hat{\epsilon}_r = 78$, and the conductivity is set as $\sigma = 1.59\,\mathrm{S/m}$ (normal saline's material

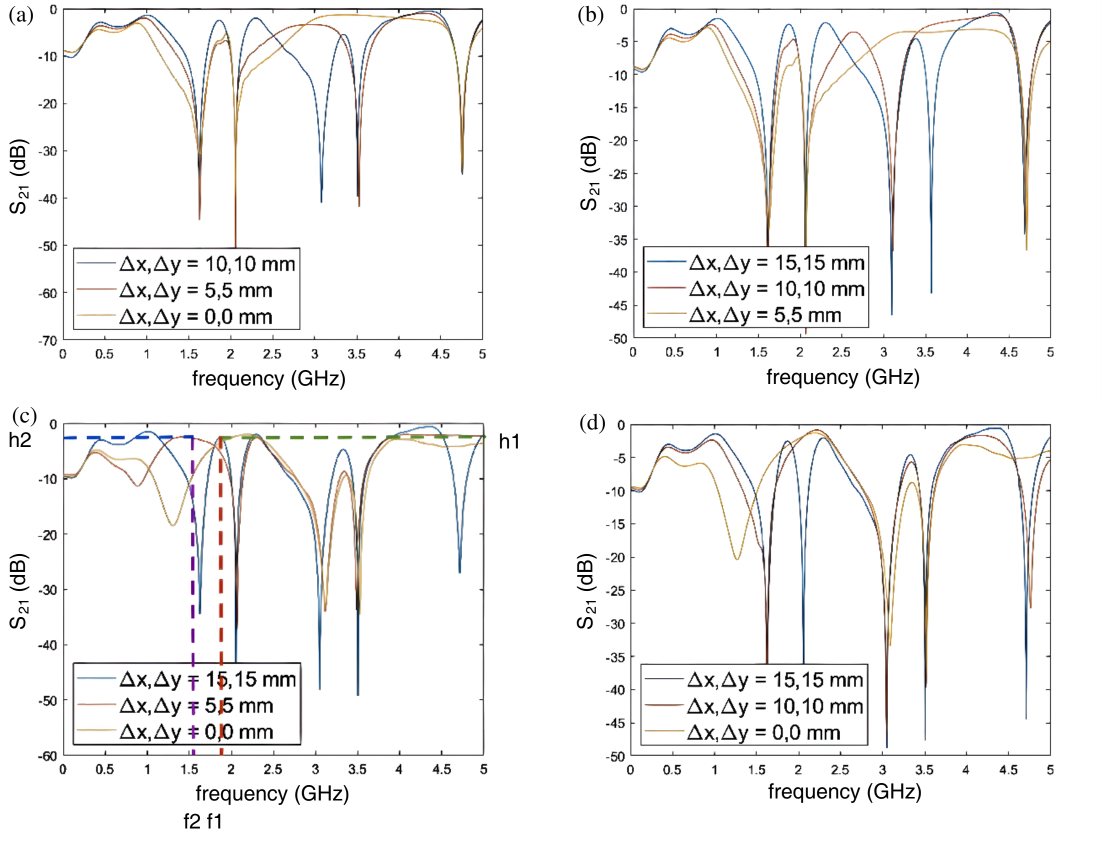

FIGURE 5. (a) Approach the center of pair1 in branch11's direction. (b) Approach the center of pair1 in branch12's direction. (c) Approach the center of pair2 in branch21's direction. (d) Approach the center of pair2 in branch22's direction.

parameters). Then, various simulations are taken in different closing orientations to figure out the tendency of EIT bands to alter while the position of the cylinder changes.

These two narrow EIT bands are generated by two pairs of open stubs respectively, and each amplitude dip of a single EIT band is attributed to one open specific stub. This is because the transmitted signal has to experience an extra phase shift during propagation, and the resonance point is changed consequently. More specifically, for pair1 which generates the EIT peak at 3.4 GHz, branch11 induces the left dip, and branch12 induces the right dip; for pair2 which generates the EIT peak at 1.8 GHz, branch21 induces the left dip, and branch22 induces the right dip.

As shown in Figure 5(a), when the target approaches the smallest branch11, the peak of the higher EIT frequency band shifts leftward until it disappears, while the lower EIT frequency band exhibits a slight decrease in amplitude. As depicted in Figure 5(b), when the target approaches branch12, the peak of the higher EIT frequency band shifts leftward more noticeably until it vanishes, and the lower EIT frequency band also shows a slight decrease in amplitude. Simultaneously, as the target approaches branch21 (Figure 5(c)), the peak of the lower EIT band shifts noticeably to the left, and the higher EIT band shows a slight decrease in amplitude. As shown in Figure 5(d), when the target approaches the largest branch22, the peak of the lower EIT band shifts more noticeably to the left compared to Figure 5(c), and the higher EIT band also exhibits a slight decrease in amplitude. For the key values required in Equation (2), Figure 5(c) marks the center frequency f_1 and its amplitude value h_1 at a 15 mm offset around the significantly changed lower EIT frequency band when the target is near branch21, along with the center frequency f_2 and its amplitude value h_2 at a 5 mm offset.

4. EXPERIMENTS

The printed circuit board (PCB) of the touch sensing planar circuit structure is designed and fabricated as in Figure 6(a). Figure 6(b) illustrates the experimental setup used for the S-parameter measurements, including the Vector Network Analyzer (VNA) connection scheme and the placement of the sensing board, which ensures consistent measurement conditions across all test cases. Figure 6(c) shows the difference between the simulated and experimental results. These two waves are generally consistent with each other except slight ripples and decrease on amplitude resulted by the bias on actual parameters because of non-ideal experimental environment. As for deviation from the original simulation result of the schematic, it is mainly because in the ADS simulation, ideal transmission line is used, and only equivalent parameters in transvers direc-

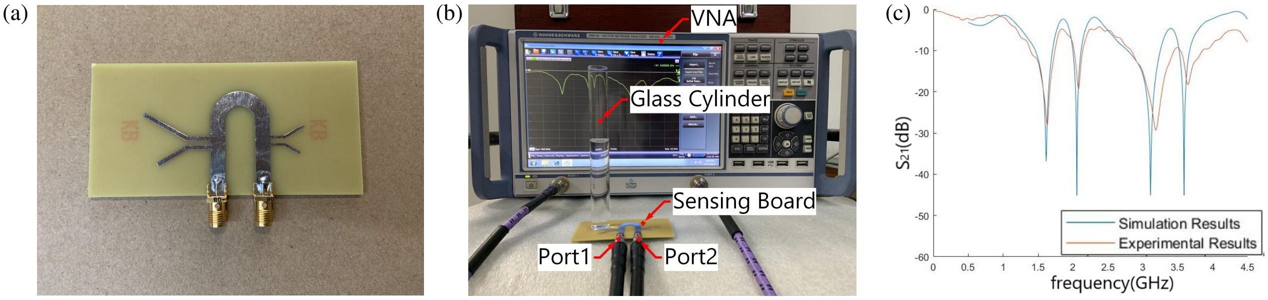

FIGURE 6. (a) Sensing board. (b) Experiment devices. (c) Comparison of S_{21} results between simulation and experiment.

tion are considered, which lead to deviation in specific structure parameters.

In addition, the equivalent-circuit simulation shows good agreement with the full-wave EM simulation, particularly in the resonance frequencies. This is because the $ABCD$ parameters used in the circuit model were extracted from ADS based on the effective microstrip characteristics, rather than derived from idealized transmission-line formulas. The small discrepancies between the two simulations are mainly caused by discontinuities at the microstrip's tub junctions and the mutual coupling among the parallel branches, which are fully captured in EM simulation but only partially reflected in the simplified circuit model. These differences are minor, confirming that the proposed circuit analysis accurately represents the essential behavior of the implemented structure. By utilizing the variation of the EIT bands under capacitive loading, the position of the loading source can be precisely determined.

In order to describe the relationships between the position of cylinder and the change of S_{21} waveform (both amplitude and frequency), a numerical measurement named shifting vector is proposed. The shifting vector is a 1×3 vector consisting of three elements p_f, p_a, and p_n, where p_f is the difference of EIT peak's central frequency between the original EIT band and the one interfered by the placement of cylinder; p_a is the difference of EIT peak's linear amplitude between the original EIT band and the one interfered by the placement of cylinder; p_n is the EIT band number used to distinguish those two EIT bands. For instance, the EIT band induced by pair2 is labeled with $p_n = 2$. In this way, every shifting vector is able to be representative for a certain position of the cylinder and will be used for further analysis. To make a more specific explanation, for open stubs using the data given in Figure 4, the shifting vector is defined as

$$SV = [p_n, p_a, p_f] = \left[2,\ 10^{\frac{h_1}{20}} - 10^{\frac{h_2}{20}},\ 10^{\frac{f_1}{20}} - 10^{\frac{f_2}{20}}\right] \quad (2)$$

where h_1 and h_2 are actually the value of S_{12} in the form of dB. f_1 and h_1 are the central frequency and amplitude of pair2's original left EIT peak; f_2 and h_2 are the central frequency and amplitude of the identical but altered EIT peak when the cylinder is placed at 5 mm away from the center of pair2 along branch21's direction. The constant 20 is a normalization factor used for balancing amplitude and frequency components.

Then, the sensing board plane is divided into unit squares with side length 3 mm for locating the position of cylinder by the SV (shifting vector). The cylinder is placed at every grid point with its axis of symmetry exactly aligning with that point, and the corresponding shifting vector is measured and calculated. To explore the latent relationship between the shifting vector and the real position of the cylinder, a complex form $p_f + jp_a$ is then put forward to represent the shifting vector, where p_f and p_a are defined as above to represent the extent of S_{21} waveform change. The magnitude and phase spectrums of this complex value are plotted for each of the two open stub pairs separately in Figure 7, using the values transferred from the acquired shifting vector at every lattice point, and the p_n parameter in the shifting vector can thus be ignored.

In order to examine the accuracy of the measurement model, the utilization of these two spectrums is further advanced in the following analysis. The cylinder is randomly placed in the grid area (not at the lattice points to improve robustness) with the shifting vector calculated and transferred into the forms of magnitude and phase. Since the plane of the sensing structure is divided into squares, every region is represented by its four vertexes' grid number. Those two transferred values (magnitude and phase) from the shifting vector of its real position and the range of values bounded by the region (lattice values of the region in the spectrums) are used for locating the specific region of the cylinder. If the magnitude value and phase value project to the same and unique region, namely either of these two values is in range of value mapped from the only identical region to the corresponding spectrum, we can claim that it hits and regard it as a positive sample; otherwise if the magnitude and phase values project to different regions, or there are more than one region satisfy the value limits, it fails or is regarded as a negative sample. The accuracy of this design, which is acquired by division of the positive sample number and the total sample number, can reach 94.4% in 54 random location samples. This accuracy represents the achievable level under current fabrication and algorithmic conditions. It is convinced that this design has huge potential for applications such as precise touch localization.

At the same time, its frequency selective capability provides a filtering function, allowing signal transmission within passbands that are not sensitive to sensing. It also has the potential to enable compatibility with multiband filter designs in radio-frequency communication circuits.

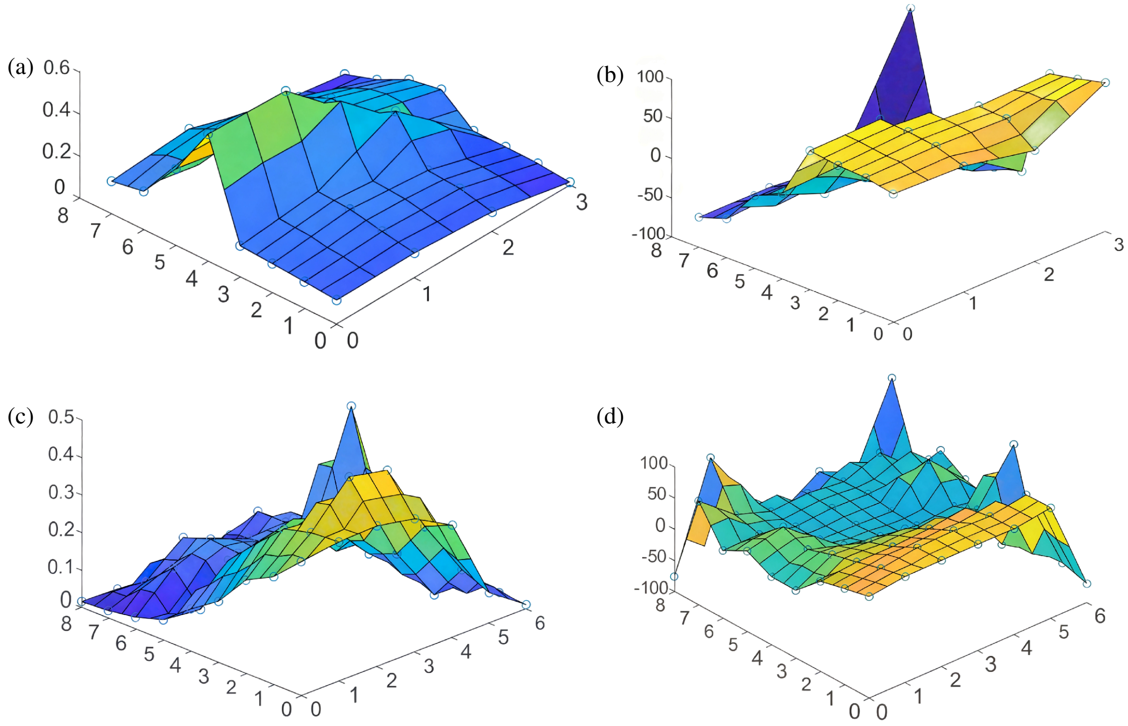

FIGURE 7. (a) Magnitude spectrum of left pair. (b) Phase spectrum of left pair. (c) Magnitude spectrum of right pair. (d) Phase spectrum of right pair.

The existing EIT designs and touch sensing methods differ significantly from this work. Refs. [12] and [13] employ waveguide resonators to achieve EIT and Fano resonance near 3 GHz, where the resonant frequency shift correlates with changes in the waveguide medium's dielectric constant. This design focuses solely on structural variations and lacks sensing capability. Ref. [16] proposes a miniaturized microwave dielectric constant sensor based on EIT, featuring broad measurement capability near 2.64 GHz. Both its microstrip and sensing structures have centimeter-scale dimensions. The additional sensing structure near EIT microstrip transmission lines is designed for dielectric property characterization, not for interactive or position-resolved sensing. Ref. [17] reports a multiband EIT-like microstrip structure designed to enhance resonant response from 5 GHz to 25 GHz through millimeter-scale structures. However, this structure exhibits no two-dimensional positioning or interactive touch sensing capabilities and lacks compatibility with RF circuits. The dual-band EIT microstrip design proposed herein overcomes these limitations by enabling position sensing without additional components while maintaining RF transmission capability.

5. CONCLUSION

In this work, an EIT-based microstrip structure and a numeric representation of frequency and amplitude shift (the shifting vector) were proposed. The basic tendency of the S-parameter variation caused by the movement of finger-like dielectric or conductive objects was identified and quantified. Unlike conventional touch-sensing approaches that rely on additional sensing components, the proposed method integrates the sensing function directly into the existing RF microstrip line. This design allows interactive touch detection to be realized without introducing any extra sensor devices, ensuring that the RF communication and transmission performance of the system remain unaffected. By employing the shifting vector, the proposed system achieves a touch localization accuracy of 94.4% with millimeter-level resolution. The results validate the feasibility of using an EIT-based microstrip as a low-cost, multifunctional platform that combines RF communication and interactive sensing in a single structure. Future work will focus on improving localization accuracy through continuous position tracking and integrating machine-learning algorithms for gesture recognition, further expanding its applicability in low-cost intelligent RF interactive systems.

ACKNOWLEDGEMENT

The authors wish to acknowledge the contribution of Yunhao Fang from Zhejiang University, whose participation and support greatly enhanced the quality of this research.

REFERENCES

[1] Papasimakis, N. and N. I. Zheludev, "Metamaterial-induced transparency: Sharp Fano resonances and slow light," *Optics and Photonics News*, Vol. 20, No. 10, 22–27, 2009.

[2] Lukin, M. D. and A. Imamoğlu, "Controlling photons using electromagnetically induced transparency," *Nature*, Vol. 413, No. 6853, 273–276, 2001.

[3] Hamedi, H. R., J. Ruseckas, and G. Juzeliūnas, "Exchange of optical vortices using an electromagnetically-induced-transparency-based four-wave-mixing setup," *Physical Review A*, Vol. 98, No. 1, 013840, Jul. 2018.

[4] Amin, M., R. Ramzan, and O. Siddiqui, "Slow wave applications of electromagnetically induced transparency in microstrip resonator," *Scientific Reports*, Vol. 8, No. 1, 2357, 2018.

[5] Alzar, C. L., M. A. G. Martinez, and P. Nussenzveig, "Classical analog of electromagnetically induced transparency," *American Journal of Physics*, Vol. 70, No. 1, 37–41, 2002.

[6] Sundaravadivel, P., S. Thangavel, G. B. P. Jegajothi, R. Meenakshi, D. S. S. Raja, and D. R. Kumar, "A high-performance, thin, circularly polarized microstrip antenna for compact radar systems," *Progress In Electromagnetics Research Letters*, Vol. 124, 31–36, 2025.

[7] Liu, S., Z. Xu, X. Yin, and H. Zhao, "Analog of multiple electromagnetically induced transparency using double-layered metasurfaces," *Scientific Reports*, Vol. 10, No. 1, 8469, 2020.

[8] Chiam, S.-Y., R. Singh, C. Rockstuhl, F. Lederer, W. Zhang, and A. A. Bettiol, "Analogue of electromagnetically induced transparency in a terahertz metamaterial," *Physical Review B*, Vol. 80, No. 15, 153103, 2009.

[9] López-Tejeira, F., R. Paniagua-Domínguez, and J. A. Sánchez-Gil, "High-performance nanosensors based on plasmonic Fano-like interference: Probing refractive index with individual nanorice and nanobelts," *ACS Nano*, Vol. 6, No. 10, 8989–8996, 2012.

[10] Wu, C., A. B. Khanikaev, R. Adato, N. Arju, A. A. Yanik, H. Altug, and G. Shvets, "Fano-resonant asymmetric metamaterials for ultrasensitive spectroscopy and identification of molecular monolayers," *Nature Materials*, Vol. 11, No. 1, 69–75, 2012.

[11] Touiss, T., I. E. Kadmiri, Y. Errouas, and D. Bria, "Electromagnetically induced transparency and Fano resonances in waveguides and U-shaped or cross-shaped resonators," *Progress In Electromagnetics Research M*, Vol. 127, 53–63, 2024.

[12] Khattab, M. S., T. Touiss, I. E. Kadmiri, F. Z. Elamri, and D. Bria, "Multi-channel electromagnetic filters based on EIT and fano resonances through parallel segments and asymmetric resonators," *Progress In Electromagnetics Research Letters*, Vol. 115, 105–109, 2024.

[13] Wang, F., J. Cui, H. Liu, T. Ma, X. Wang, and Y. Liu, "Terahertz metamaterial devices with switchable absorption and polarization conversion based on vanadium dioxide," *Progress In Electromagnetics Research C*, Vol. 153, 61–70, 2025.

[14] Ennasar, M. A., M. E. Khamlichi, Y. Akazzim, A. Tachrifat, M. Aznabet, O. E. Mrabet, and M. Khalladi, "Design and integration of a flexible RFID UHF antenna with a 3D printed fluid channel for liquids sensing applications," *Progress In Electromagnetics Research C*, Vol. 157, 65–73, 2025.

[15] Liu, S. and F. Xue, "Miniaturized and wide-range microwave-permittivity sensor based on electromagnetic-induced transparency," in *Photonics*, Vol. 12, No. 3, 283, 2025.

[16] Liu, S., R. Ning, J. Zhu, and Y. Zhang, "Multiband electromagnetically induced transparency-like on metamaterials," *Optics Communications*, Vol. 574, 131065, 2025.

[17] Ye, H.-N., B.-F. Wan, and H.-F. Zhang, "The realization of broadband electromagnetically induced transparency metastructure based on the resonance between dielectric ceramic and metal," *Ceramics International*, Vol. 50, No. 17B, 31 235–31 248, 2024.

[18] Siddiqui, O. F., "The forward transmission matrix (FTM) method for S-parameter analysis of microwave circuits and their metamaterial counterparts," *Progress In Electromagnetics Research B*, Vol. 66, 123–141, 2016.